Geometric characteristics of bicuspid aortic valves

Jan Nijs, MD,[a,b] Babs Vangelder, MD,[c] Kaoru Tanaka, MD PhD,[b,d] Sandro Gelsomino, MD, PhD, FESC,[a,e] Ines Van Loo, MD,[a] Mark La Meir, MD, PhD,[a,e] Jos Maessen, MD, PhD,[e,f] and Bas L. J. H. Kietselaer, MD, PhD[g]

ABSTRACT

Objective: We studied the coaptation angles α and β in bicuspid aortic valve geometry from computed tomography scan images.

Methods: In 45 patients, we calculated the coaptation angle α (the angle between the nonfused commissures crossing the center of coaptation), angle β (between the nonfused commissures crossing the center of the reference circle), angles γ_1 and γ_2 and ε_1 and ε_2 (angle between the nonfused commissures and the coaptation point at the raphe or the perfect midpoint, respectively), the length of the raphe, the absolute and relative sinuses' surfaces (relative to the perfect circle and the percentage exceeding the ideal circle). Spearman correlation was employed to investigate the associations among all parameters.

Results: The coaptation angles α and β were significantly different ($P < .001$). We found a significant correlation of α with the length of the raphe ($P = .008$), whereas β was dependent on the position of the commissures. Both γ_1 and γ_2 ($P = .04$), or ε_1 and ε_2 ($P < .001$) significantly differed from each other and ε_2 was the most constant angle, although its size geometrically depends on β. The noncoronary was the largest sinus, and β was the primary determinant of its increased size in bicuspid aortic valves with righ/left fusion pattern.

Conclusions: The coaptation angle α is influenced by the length of the raphe, whereas angle β is dependent on the position of the commissures. The position of the raphe can vary and is not always situated in the middle of the free edge. The position of the right/non commissure is variable, whereas the right/left commissure is more fixed. (JTCVS Techniques 2021;10:200-15)

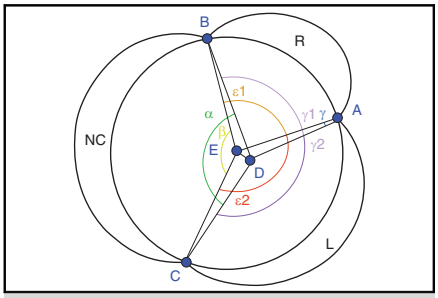

Summarization of the main features of the article.

CENTRAL MESSAGE

In BAV with complete fusion, the commissural orientation is determined by a variable combination of commissural position and length of the raphe.

PERSPECTIVE

The coaptation angle α, influenced by the length of the raphe, does not reflect the correct position of the commissures dictated by the commissural angle β. For repair, preferably both angles should be considered separately. The orientation of the raphe and position of R/N commissure are variable. The noncoronary sinus was the largest that increases with β.

See Commentaries on pages 216 and 217.

From the [a]Cardiac Surgery Division, Department of Cardiac Surgery, [b]Department of Cardiac Surgery, Brussels Center for Aortic and Cardiovascular Connective Tissue Diseases, [c]Cardiology Division, Department of Cardiology, and [d]Cardio-Radiology Division, Department of Radiology, University Hospital Brussels, Brussels, Belgium; [e]Cardiothoracic Surgery Division, Cardiovascular Research Institute Maastricht, [f]Cardiothoracic Surgery Division, Department of Cardiothoracic Surgery, and [g]Cardiology Division, Department of Cardiology, Maastricht University Medical Centre, Maastricht, The Netherlands.

Received for publication Nov 18, 2020; accepted for publication Aug 19, 2021; available ahead of print Aug 27, 2021.

Address for reprints: Jan Nijs, MD, Department of Cardiac Surgery, University Hospital Brussels, Laarbeeklaan 101, 1090 Jette, Belgium (E-mail: jannijs71@gmail.com).

2666-2507

https://doi.org/10.1016/j.xjtc.2021.08.032

▶ Video clip is available online.

The bicuspid aortic valve (BAV) is the most common congenital cardiac malformation, affecting approximately 1% to 2% of the general population,[1-6] Its main anatomic feature is the consequence of anomalous embryologic development[6] resulting in 2 functional commissures of normal height (bicommissural valve) with a third rudimentary commissure varying in height and present in approximately 95% of cases.

BAV affects the aortic root, ascending aorta, or aortic arch in about 70% of patients,[3] and it is among the most

Abbreviations and Acronyms
BAV = bicuspid aortic valve
CT = computed tomography
NCS = noncoronary sinus

common causes of aortic stenosis, aortic dilatation,[3,5,7] and aortic regurgitation,[7,8] frequently requiring surgical intervention.[9-11] Moreover, because BAV often affects individuals in their third and fourth decades of life, operative decision making is challenging in these patients and the appropriate choice among the alternative possibilities of treatment is still an area of concern and debate.[8,12]

During the past decade, interest in aortic valve repair has increased[10,13,14], as has knowledge that a detailed understanding of the morphology and function of the BAV are necessary to obtain a successful and durable repair.[10] Because the BAV morphology is complex, anatomical variations often occur that have not been completely analyzed. It is, therefore, necessary to have an even more in-depth insight into BAV structures.

Although a commissural orientation (coaptation angle α) $>150^\circ$ obtained through repositioning of the nonfused commissures has been advocated to increase the durability of the surgical repair,[5] we hypothesize that the relationship between the coaptation angle and the position of the nonfused commissures is not constant.

This study describes a new methodology for examining the BAV geometrical characteristics and is aimed at investigating the relation between the exact position of the commissures and the coaptation angle α, discussing their potential influence on surgical valve repair.

METHODS

Due to the retrospective nature of the study, ethical committee approval was waived for. The patients gave their written consent to the intervention and, at the same time, their approval the use of data for scientific purposes.

Patients

Consecutive patients with a diagnosed BAV undergoing a cardiac computed tomography (CT) or a preoperative CT of the thoracic aorta between 2008 and 2015 were included in the study. All cardiac CT imaging procedures where electrocardiography-triggered. Reasons for exclusion were significant motion artifacts.

CT Examination and Measurements

All patients underwent cardiac CT studies or CT scans of the thoracic aorta. Triggered diastolic images were taken at 75% of the RR-interval on average. Raw data were used for the analysis. All CT scans were searched for the ideal image plane, clearly showing the aortic valve cusps, their free margins, the raphe, and the nonfused commissures. Optimal diastolic images without motion artifacts were selected manually. Geometrical parameters were measured in diastolic images. For this purpose, 2 different commercially available software systems were used: IMPAX (Agfa, Mortsel, Belgium), IntelliSpace (Philips, Eindhoven, the Netherlands) and Syngo Via (Siemens, Erlangen, Germany). The same observer performed all CT measurements 2 times. Figure E1 describes the methodology to create the desired image plane. Geometrical parameters were used to analyze the asymmetric morphology in BAVs employing GeoGebra software (https://www.geogebra.org).

The following geometric parameters were measured:

A. The length of the raphe (Figure 1, *A* and *B*).
B. The absolute sinus surfaces (Figure 1, *C* and *D*) to evaluate the morphological trend of sinuses within the bicuspid asymmetry. This enabled us to determine the contribution of each sinus to the total aortic sinus surface and to assess their correlation with other parameters.
C. Relative sinus surface, which is the corresponding surface compared with a reference circle with a fixed radius and center E (Figure 1, *E* and *F*) and was given as a percentage of each sinus exceeding the reference circle. Three fixed points were placed at the level of maximum sinus dimensions (points J, G, and H). Then another series of three fixed points were placed on the created circle on the corresponding lines toward J, G, and H, respectively named I, K, and L. The distance |GK|, |HL|, and |IJ| were measured. The other 3 lines were drawn between I, K, and L and the center of the circle E (segments |IE|, |KE|, and |LE|), and the sections were measured. The left relative sinus was obtained as |HL|/HE. Similarly, the relative surfaces of the other sinuses were calculated as |GK|/GE and |IJ|/IE, for the right and noncoronary sinsues (NCS), respectively.
D. The coaptation angle α[7,8]: The angle between 2 lines drawn from nonfused commissures to the coaptation midpoint (Figure 2, *A* and *B*).
E. The angle β: The angle between 2 lines drawn from 1 nonfused commissure and the center point of the perfect circle created (Figure 2, *C* and *D*).
F. The angle γ: The angle between the raphe, and a line drawn between the commissures and the perfect midpoint (Figure 2, *E* and *F*). Angles γ_1 and γ_2 were comprised between each of the nonfused commissures and the raphe toward the coaptation midpoint.
G. Angles ε_1 and ε_2 (Figure 2, *G* and *H*): The angles between lines drawn from nonfused commissures on 1 hand and fused commissure on the other hand toward the perfect midpoint. Together with β, they were used to determine position consistency between commissures. To confirm the hypothesis of the fixed position of the commissures between the right and the left cusp, and the left and the noncoronary cusp, ε_2 should be a constant.
H. Aortic dimensions. Aortic annulus, aortic root, sinotubular junction, ascending aorta, and the aortic arch were measured. The aortic annulus was determined following the Society of Cardiovascular Computed Tomography guidelines.[15,16] Figure E2 shows the method used in the case of the BAV with only 2 sinuses.

DATA ANALYSIS

The distribution of continuous variables was defined by using the Shapiro-Wilk test. According to the results of the test, continuous data were expressed as median $\pm$ interquartile range difference. Comparisons were carried out by the Wilcoxon signed-ranked test, Mann-Whitney *U* test, and Kruskal-Wallis test. Spearman rho was employed to investigate bivariate correlations between various continuous parameters. Intrarater reliability was analyzed by calculating intraclass correlations and applying the Bland-Altman plot, as shown in Figure E3 and E4. SPSS software version 22.0 (IBM-SPSS, Inc, Chicago, Ill) was used for all calculations.

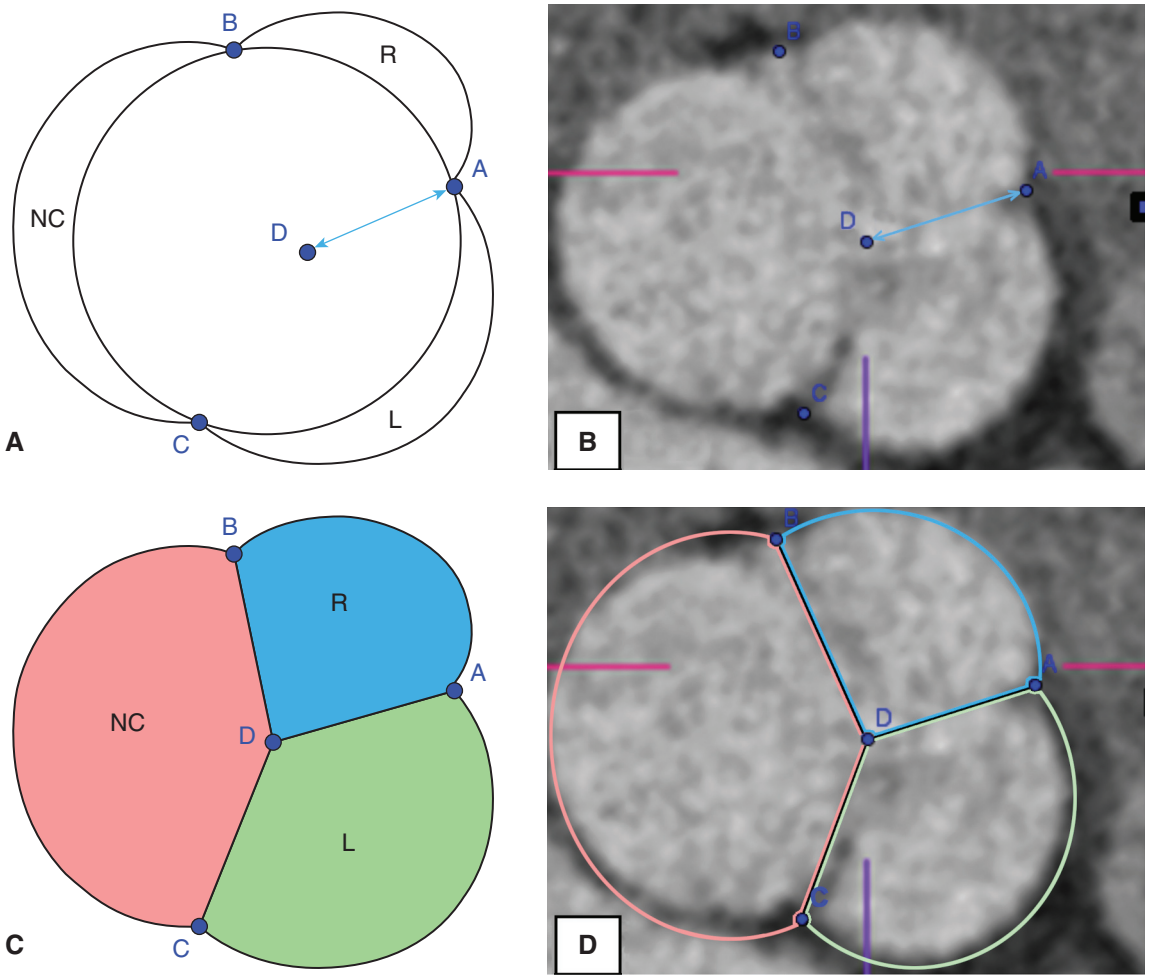

FIGURE 1. Schematic of raphe and sinus measurements from computed tomography scan. A and B, Measurement of the length of the raphe. The length of the raphe |AD| was measured as the distance between from the external point of the raphe A and the coaptation midpoint D. C and D, Sinuses' surface. Three segments were drawn: the length of the raphe |AD| as described above; a line between the nonfused commissure B, and the coaptation midpoint D (segment |AD|); and A line between the nonfused commissure A and the coaptation midpoint D, segment |BD|). These 3 lines defines the extension of the three sinuses (noncoronary [*NC*], right coronary [RC], and left coronary [LC]). Once the sinuses were defined, their surfaces were measured. E and F, Relative sinuses' surface. For these measurements, a circle was drawn passing through the position of the raphe A, the position of the non-fused commissure B, and the position of the nonfused commissure C, and its center E was identified. Three fixed points were placed at the level of maximum sinus dimensions (points J, G, and H, respectively). Then another series of 3 fixed points were placed on the created circle, respectively named I, K, and L. The distance |GK| was the difference (protrusion) between the midpoint of the RC sinus and its projection on the created circle. Similarly, the segment |HL| was the difference between the midpoint of the LC sinus and its projection on the created circle and the distance |IJ| was the difference between the midpoint of the NC sinus and its projection on the created circle. These distances were measured as the differences between the distances from single sinuses midpoints (G, H, and J for the RC, LC and NC, respectively) and the circle center E and the distances from single sinus midpoint projection on the circle (K, L, and I for the RC, LC, and NC, respectively). Finally, the amount of sinus protrusion was calculated as the ratio between these distances. For the RC it was: $|GK|/(|GK| + |KE|) = |GK|/GE$. Similarly, the protrusion of LC was calculated as: $|HL|/(|HL| + |LE| = |HL|/HE$ and the protrusion of NC was calculated as: $IJ|/(|IJ| + |JE|) = |IJ|/IE$, for the LC and NC, respectively.

RESULTS

Patient Population

The study population consisted of 45 patients. Baseline patient characteristics are shown in Table 1. All patients had congenital BAV, of which 35 (77.8%) had an right/left fusion pattern. The most prevalent aortic pathology was a supracoronary ascending aortic aneurysm (n = 27 [60%]). The aorta was unaffected in 13% (n = 6).

General CT Features

CT imaging characteristics are shown in Table 2. In 53.3% of patients, a calcified aortic valve was found. 91.1% of the valves consisted of 3 sinuses, of which the NCS was the largest. Seventy-seven percent of patients had normal anatomy of the aortic arch. One patient was diagnosed with a bovine arch, in 1 other patient an aberrant right subclavian artery was found. Table E1 shows that

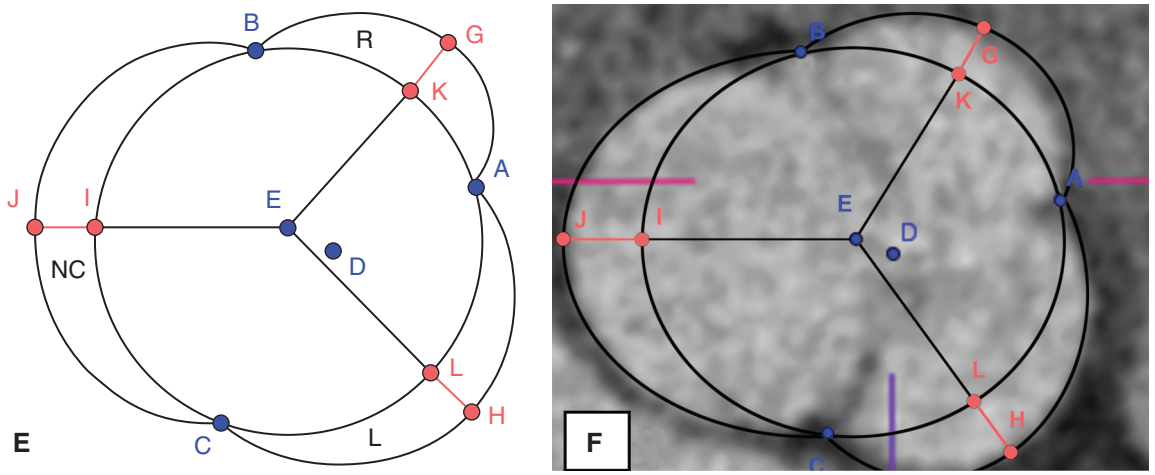

FIGURE 1. (Continued).

excluding the ascending aorta, the aortic dimensions were larger in men than in women. Furthermore, 2-sinus valves showed larger aortic root, sinotubular junction, and ascending aorta diameters. In contrast, aortic dimensions did not significantly vary between valves with different cusp fusion patterns.

Geometrical Measurements

The measured geometric parameters are shown in Table 3. The α and β angles were significantly different ($P < .001$). The median angle difference was 15°with a maximum difference of 47° and a minimal difference of 1.4°. This difference was significantly higher in the 3-sinus group ($P = .009$), whereas it was not different between BAV with varying cusp fusion patterns ($P = .28$). The angles γ_1 and γ_2 were statistically different ($P = .04$) and the median commissural orientation $\varepsilon 1$ differed from ε_2 ($P < .001$). From all calculated commissural positions, ε_2 appeared to be the most constant angle.

Looking at the relative size of each sinus beyond the radius of the reference circle, the NCS appeared to be the largest sinus (+16.7% ± 6.67%). In contrast, the right coronary sinus had the smallest percentages with a median increase of +10.71% ± 4.63% compared with the perfect circle.

Correlation Analysis

A moderate correlation (Table 4) was found between the length of raphe and the angle α ($P = .008$), whereas there was no correlation with β ($P = .548$). Moreover, $\Delta\alpha\beta$ significantly correlated with and the distance between the commissural point and the reference center $|DE|$ ($P < .001$) as well as with $\Delta\,|AE||AD|$ ($P < .001$). In contrast, both $\Delta\gamma_1$ and γ_2 showed no correlation with $\Delta\alpha\beta$. There was a slight inverse correlation between the 3 sinus surfaces and $\Delta\alpha\beta$ ($P = .01$ and .02 and $P = .017$, in left coronary sinus, right coronary sinus, and NCS, respectively) and a small direct relationship between the NCS surface and β ($P = .03$).

When analyzing the correlations between the relative sinus sizes and all geometrical parameters (Table 5), we observed that the left sinus surface showed a moderate correlation that was inverse with β ($P = .007$). At the same time, it was directly correlated to $\Delta\alpha\beta$ ($P = .001$), $\Delta\gamma_1\gamma_2$ ($P = .001$) $\Delta\varepsilon_1\varepsilon_2$ ($P = .01$), and $|DE|$ ($P < .001$). In addition, the right sinus surface significantly inversely correlated with $\Delta\alpha\beta$ ($P = .001$). Finally, we failed to find any significant correlation between the noncoronary sinus surface and the other parameters.

INTRAOPERATOR VARIABILITY

The intraclass correlation was >0.9 for all measurements ($P < .001$), as shown in Table E2. The mean differences between the 2 measures were small and all close to zero and a good agreement at regression. The Bland-Altman plots are shown in Figure E3 and E4. Overall, the interrate variability was small, and the agreement between measurements was high.

DISCUSSION

Aortic valve repair is a preferred option for patients with BAV because of its advantages over valve replacement.[12] To choose the best repair strategy, advanced assessment of the geometric characteristics of the aortic valve must be mastered by all surgeons who want to perform valve-preserving surgery.[17] Commissure orientation, defined as the angle α formed by the lines joining the commissures to the central axis of the valve, varies between 120°

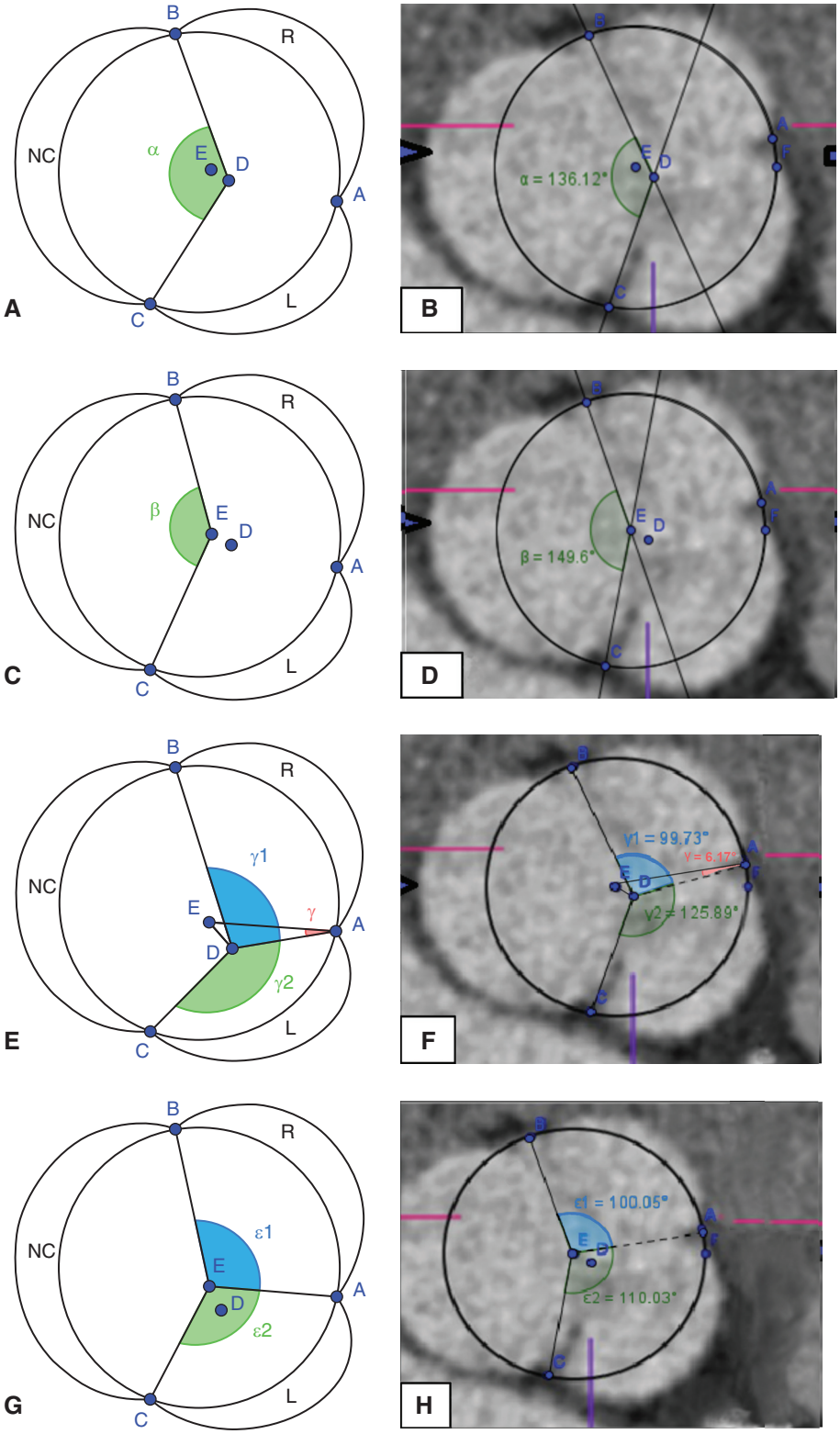

FIGURE 2. Schematic of angles' measurements from the computed tomography scan. A and B, Coaptation angle α, which is the angle between the nonfused commissures |BD| and |DC| from the bicuspid coaptation midpoint D. C and D, A circle was drawn through the position of the raphe A, the position of the nonfused commissure B, and the position of the nonfused commissure C and its center E was identified. Angle β is defined as the angle between the nonfused commissures |BE| and |DE| and center of the circle E. It represents the true commissural orientation in an ideal circle. E and F, The point E is the center of a circle drawn through the position of the raphe A, the position of the nonfused commissure B, and the position of the nonfused commissure

(tricuspid configuration) and 180° (bicuspid symmetrical shape).[17] Schäfers and colleagues[7,8] showed that a commissural orientation as close as possible to 180°, by repositioning of the nonfused commissures, increases the durability of the repair by decreasing shear stress on the cusps. Other groups reported excellent results with α of 120° or 180°.[17,18-20] In this article, we presented a new CT–scan-based method that describes the aortic valve geometry in order to increase the understanding of the geometric morphology of the BAV. We tested the hypothesis that the coaptation angle α lacks a constant relationship with the exact position of the commissures. If this hypothesis is confirmed, the angle α alone might not be solely dependent on the true position of the commissure. Considering the true commissural angle β, we observed that the coaptation angle α significantly differs from the commissural angle β ($P < .001$). This suggests that the coaptation angle α indeed lacks a constant relationship with the exact position of the commissures. This was confirmed by the observation that even when the commissures were normally or near-normally positioned a commissural orientation α of 120° to 140° can be observed.

The data showed a significant correlation of α with the length of the raphe ($P = .008$), which in contrast, did not correlate with β ($P = .58$). This finding might suggest that α is influenced by the length of the raphe rather than by the true commissural position.

Moreover, we found that the angles $\gamma 1$ and $\gamma 2$ significantly differed from each other ($P = .04$), demonstrating that in many cases the raphe is not situated in the middle of the free edge and its coaptation midpoint can vary. This finding might suggest that the orientation of the raphe also has a different influence on α and β. The variability of the raphe's orientation is confirmed by the difference between the coaptation midpoint and the perfect center point |DE|. This segment, as well as the difference between the length of the raphe versus the length between the commissure and the circle midpoint (|AE| and AD|, respectively), were significantly correlated to $\Delta\alpha\beta$ (both P values $< .001$). The coaptation angle α, on which valve repair decision making is partly based, may have no or minimal relationship with the true location of the 3 commissures, being more dependent on the length of the raphe instead. At the same time, β is dependent on the position of the nonfused commissures on a perfect circle, drawn through all 3 commissures. As a consequence, when considering the reposition of the commissures during remodeling or reimplantation, the surgeon could consider α and β separately. (Figure 3). Although midterm durability with commissural reorientation seems to be good, exact influence of this maneuver on mobility and shear stress of the fused cusp remains unknown. Further studies with 4-dimensional magnetic resonance flow imaging could help in elaborate on the effect of commissural repositioning on flow through the bicuspid valve.[21]

During valve surgery of BAV with righ/left fusion pattern it is often seen that the fused commissure, together with the commissure between the left and the noncoronary cusp, appears to be positioned at a fairly fixed point. In contrast, the commissure between the right and noncoronary cusp seems to be rather variable, mostly being displaced to the left. We hypothesized that if $\varepsilon 1$ and $\varepsilon 2$ differed from each other, this finding would demonstrate rather fixed positions of the commissures between the right and the left cusp and the left and noncoronary cusp. Angle ε_2 should be quite constant to confirm this observation. In our experience, ε_1 and ε_2 differed from each other ($P < .001$) and $\varepsilon 2$ was the most constant angle, compared with $\varepsilon 1$ and β, suggesting that the position of the right commissure is less constant. At the same time, although $\varepsilon 2$ is more fixed, its size geometrically depends on β. This reflects our experience during surgical inspection that the right:non commissure is frequently already positioned to the left. If this is correct, one might consider to only reposition the left/non commissure aiming at symmetrical fused cusp ($\varepsilon 1 = \varepsilon 2$), this without the risk of damaging the atrioventricular conduction system. However, more measurements of $\varepsilon 2$ are necessary to confirm the altered position of the commissure between the right and noncoronary cusps. This might be of clinical importance because the interleaflet triangle underneath the right and noncoronary cusp is closely related

C, whereas D is the coaptation point. The distance between these 2 central points |ED| was measured. In addition, 2 lines were drawn from the position of the raphe A to both center points E (line |AE|) and D (line |AD|) and were measured. Their difference in distance (|AE| – |AD|) was also determined and angle γ (*red*) between EAD was calculated. Two more angles were measured: the angle $\gamma 1$ (*light blue*) was the angle between the nonfused commissure B, the position of the raphe A, and the coaptation point D, obtained drawing the segments |BD| and |AD|; the angle $\gamma 2$ (*light green*) was the angle between the nonfused commissure and the position of the raphe A, obtained drawing the segments |CD| and |AD|. G and H, Reference angles. The point E is the center of a circle drawn through the position of the raphe A, the position of the nonfused commissure B and the position of the nonfused commissure C. Another 2 angles were measured: the angle $\varepsilon 1$ (*light blue*) was the angle between the nonfused commissure B, the position of the raphe A, and the circle center E, obtained drawing the segments |BE| and |AE|; the angle $\varepsilon 2$ (*light green*) was the angle between the nonfused commissure and the position of the raphe A, obtained drawing the segments |CE| and |AE|. To confirm the hypothesis of a rather constant position of the commissures between the right and the left cusp, and the left and the noncoronary cusp, $\varepsilon 2$ should be a constant. *NC*, Noncoronary.

TABLE 1. Patient characteristics (N = 45)

Characteristic	Result
Age (y)	56
Male sex	38 (84.4)
BMI	26
Hypertension	24 (53.3)
Hypercholesterolemia	17 (37.8)
Diabetes mellitus	3 (6.7)
Coronary artery disease	8 (17.8)
Chronic renal failure	1 (2.2)
Familial BAV	1 (2.2)
Marfan syndrome	0
Genetic testing	9 (20)
Cusp fusion pattern	
True bicuspid	4 (8.9)
Right/left fusion pattern	35 (77.8)
Right/non fusion pattern	5 (11.1)
Left/non fusion pattern	1 (2.2)
Aortic pathology	
None	6 (13.3)
Ascending aortic aneurism	27 (60)
Aortic coarctation	2 (4.4)
Aortic root aneurysm	5 (11.1)
Combined aneurysm	4 (8.9)
Type A dissection	1 (2.2)
Aortic valve surgery	
None	23 (51.1)
Repair	11 (24.4)
Replacement	11 (24.4)
Aortic surgical correction	
None	29 (64.4)
David	3 (6.7)
Yacoub	7 (15.6)
Perceval	2 (4.4)
Combined surgery	
Bentall	4 (8.9)
Surgical indication	
None	26 (57.8)
Aortic regurgitation	2 (4.4)
Aneurysm progression	6 (13.3)
Aortic stenosis	6 (13.3)
Aortic regurgitation + aneurysm progression	4 (8.9)
Dissection	1 (2.2)
LVEF (%)	60 (7)
LVEDD (mm)	51.5 (11.75)
Annulus diameter (mm)	28 (5)
Sinus diameter (mm)	40.75 (10.88)
Ascending aorta diameter (mm)	42 (10.75)
Aortic regurgitation grade	
None	10 (22.2)
Mild	22 (48.9)
Moderate	6 (13.3)
Serious	4 (8.9)
Aortic regurgitation type	
Unknown	19 (42.2)
Type 1 (dilatation)	12 (26.7)
Type 2 (prolapse)	4 (8.9)
Type 3 (restriction)	7 (15.6)
Maximum gradient (mm Hg)	25 (32.42)
Mean gradient (mm Hg)	15.75 (20.6)
TEE	5 (11)

Values are presented as median (interquartile range difference) or as n (%). *BMI*, Body mass index; *BAV*, biscuspid aortic valve; *LVEF*, left ventricle ejection fraction; *LVEDD*, left ventricular end diastolic diameter; *TEE*, transesophageal echocardiography.

to the membranous septum, which contains the His bundle.[22]

Another observation was that the NCS was the largest sinus, and β was the primary determinant of its increased size in righ/left BAV. Considering this in the context of aortic valve repair, in case of a dilated NCS in right/left BAV,

TABLE 2. General computed tomography features (N = 45)

	Result
Scan protocol	
Flash	38 (84.4)
Step-and-shoot	7 (15.6)
Calcified aortic valve	24 (53.3)
Cardiac cycle: % of RR-interval	75 [17]
No. of sinuses	
2	5 (11.1)
3	40 (88.9)
Aortic arch anatomy	
Unknown	8 (17.8)
Normal	35 (77.8)
Bovine arch	1 (2.2)
Aberrant right subclavian arteries	1 (2.2)
Aorta dimensions (mm)	
Annulus	27 (5)
Aortic root	39.5 (10)
STJ	32.5 (8.95)
Ascending	43 (9.75)
Aortic arch	28 (5.75)

Values are presented as median (interquartile range difference) or as n (%). *RR-interval*, Interbeat interval; *STJ*, sinotubular junction.

TABLE 3. Cusp geometry (N = 45)

	Result
Commissural positions	
α	151° (44.6°)
β	144.50° (28.0°)
γ	8.2° (1.5°)
γ_1	107.4° (22.3°)
γ_2	103.1° (18.2°)
ε_1	113.00° (22.0°)
ε_2	100.53° (13.3°)
Length of raphe (mm)	15.6 (3.95)
|DE| (mm)	0.4 (0.1)
Sinus surface (cm^2)	
LCS	6.8 (4.3)
RCS	6.95 (4.95)
NCS	8.7 (4.57)
Sinus size relative a perfect circle (% increase)	
LCS	+13.8 (5.7)
RCS	+10.7 (4.6)
NCS	+16.7 (6.7)

Values are presented as median (interquartile range difference) or as percentage (interquartile range difference). |*DE*|, Distance between the commissural point and the reference center; *LCS*, left coronary sinus; *RCS*, right coronary sinus; *NCS*, noncoronary sinus.

the Wolfe procedure (replacement of the supracoronary ascending aorta together with the dilated NCS) receives a Class IIa recommendation (level of evidence C).[12] However, considering that the size of the NCS gets bigger when β increases, one might conclude this does not necessarily indicate that the NCS is pathologically as dilated as it seems. Unfortunately, the standard size of the NCS in the case of right/left BAV is unknown. Because the aortic root is globally dilated in most of our patients, this finding suggests that the NCS could be enlarged by design in right/left BAVs, rather than being a sign of pathological dilatation. To confirm this hypothesis, more sinus measurements should be performed at an early stage of life. In Video 1, the main findings of the study are explained by 1 of the authors.

CLINICAL APPLICATION

Although the importance of these features and their clinical application, especially regarding the surgical decision making and techniques employed have to be further explored, we have started to include preoperative CT scan evaluation as described any time an aortic valve repair is planned. In Figure 4, a clinical case of a patient referred for BAV who underwent preoperative CT scan measurements and calculations is reported. CT scan, echocardiograph, and real-time measurements matched. The practice of repositioning the commissures as close to 180° as possible is being widely adopted by repair surgeons. Repositioning of the commissures (at the level of the sinotubular junction) implies the use of an annuloplasty ring inducing the same repositioning of the base of the interleaflet triangles (virtual basal ring). Indeed, if this is done only at the level of the commissures, the aortic valve is skewed by inducing alteration of the geometry of the valve. In the case shown, the patient underwent a Yacoub operation and we avoided aggressively repositioning the commissures based on the observation that the commissural position and the raphe significantly influence the coaptation angle (commissural orientation) more than previously believed and compared with the same commissural position on a virtual circle. As shown by the postrepair image, it was sufficient to pull on the commissures along the angle α to obtain a proper coaptation and an equal length of the plicated free edges. Hence, β was respected during the surgery as to not distort the valve.

Limitations of the Study

Our study presents some limitations that must be pointed out. First, the lack of a control group to confirm the correctness of the used measurements. Second, only 1 operator took the measurements. Although the method was proven to be reliable with an intraclass coefficient >0.90, a second observer and the calculation of interobserver agreement would have strengthened the study. Third, 2 different imaging software was used, and their equivalence was not tested, examining the same CT image using both software. Fourth, although unlikely, at present it is unknown whether the commissural position changes during progressive dilatation of the aortic root or even ascending aorta. Fifth, the potential of this method to improve the possibility of valve repair has to be deeply explored because about 50% of patients did not undergo surgery. Therefore, more patients in the valve repair group are necessary to correlate the BAV aortic geometry and the surgery decision making. Finally, the CT scan images are static, and they only assess structure, rather than function. In addition, CT images only assess structure at a single time point in the cardiac cycle. To study in a static state in diastole was decided to be able to make a comparison to the commissural orientation as described in the literature. Finally, most of the preoperative necessary information, necessary to judge repairability, comes from echocardiographic diastolic images (short and long axis images, +/- color flow).

CONCLUSIONS

The coaptation angle is dependent on both the commissural position and the length of the raphe. Considering the

TABLE 4. Correlation analysis

Variable	Spearman rho	Correlation coefficient	*P* value	95% confidence interval
Length raphe	α	0.412	.008	0.119 to 0.644
	β	0.097	.584	0.211 to 0.381
	Raphe length	−0.112	.487	−0.403 to 0.217
$\Delta\alpha\beta$	|AD|	0.265	.079	−0.095 to 0.554
	|AE|	−0.152	.319	−0.450 to 0.156
	Δ |AD||AE|	0.713	<.001	0.498 to 0.862
	|DE|	0.715	<.001	0.483 to 0.853
	$\Delta\gamma_1\gamma_2$	0.171	.325	−0.181 to 0.493
LC sinus surface	α	0.118	.438	–0.192 to 0.414
	β	0.194	.201	−0.099 to 0.486
	$\Delta\alpha\beta$	−0.356	.016	−0.604 to −0.054
	$\Delta\gamma_1\gamma_2$	0.036	.837	−0.283 to 0.337
	$\Delta\varepsilon_1\varepsilon_2$	−0.269	.074	−0.555 to 0.011
	Raphe length	0.043	.789	−0.241 to 0.323
RC sinus surface	α	−0.116	.475	−0.428 to 0.218
	β	0.025	.880	−0.302 to 0.316
	$\Delta\alpha\beta$	−0.348	.028	−0.595 to −0.032
	$\Delta\gamma_1\gamma_2$	0.066	.713	−0.291 to 0.411
	$\Delta\varepsilon_1\varepsilon_2$	0.059	.719	−0.275 to 0.367
	Raphe length	0.010	.953	−0.282 to 0.308
NC sinus surface	α	0.174	.254	−0.146 to 0.457
	β	0.321	.031	0.007 to 0.544
	$\Delta\alpha\beta$	−0.353	.017	−0.607 to 0.049
	$\Delta\gamma_1\gamma_2$	−0.014	.937	−0.297 to 0.290
	$\Delta\varepsilon_1\varepsilon_2$	−0.144	.345	−0.449 to 0.168
	Raphe length	0.063	.697	−0.221 to 0.342

Values are presented as median (interquartile range difference) or as n (%). |*AD*|, Distances from nonused commissures to the coaptation point; |*AE*|, distances from nonfused commissures to the perfect central point; |*DE*|, distance between the commissural point and the reference center; *LC*, left coronary; *RC*, right coronary; *NC*, noncoronary.

TABLE 5. Relative sinus sizes: Correlation analysis

Variable	Spearman rho	Correlation coefficient	*P* value	95% confidence interval
LC sinus surface	α	−0.266	.077	−0.578 to 0.102
	β	−0.396	.007	−0.652 to −0.092
	$\Delta\alpha\beta$	0.464	.001	0.180 to 0.671
	$\Delta\gamma_1\gamma_2$	0.338	.047	0.016 to 0.596
	$\Delta\varepsilon_1\varepsilon_2$	0.360	.015	0.033 to 0.614
	Raphe length	−0.261	.100	−0.518 to 0.047
	|DE|	0.548	<.001	0.308 to 0.731
RC sinus surface	α	−0.050	.742	–0.356 to 0.230
	β	0.146	.338	–0.166 to 0.442
	$\Delta\alpha\beta$	−0.392	.008	−0.632 to −0.108
	$\Delta\gamma_1\gamma_2$	0.132	.449	−0.231 to 0.457
	$\Delta\varepsilon_1\varepsilon_2$	−0.198	.192	−0.526 to 0.145
	Raphe length	0.273	.084	−0.073 to 0.556
	|DE|	−0.252	.094	−0.497 to 0.062
NC sinus surface	α	−0.007	.964	−0.278 to 0.275
	β	−0.228	.132	−0.509 to 0.127
	$\Delta\alpha\beta$	0.075	.625	−0.257 to 0.401
	$\Delta\gamma_1\gamma_2$	0.123	.483	−0.229 to 0.454
	$\Delta\varepsilon_1\varepsilon_2$	0.075	.623	0.196 to 0.329
	Raphe length	0.116	.470	−0.238 to 0.415
	|DE|	0.144	.346	−0.189 to 0.450

LC, Left coronary; |*DE*|, distance between the commissural point and the reference center; *RC*, right coronary; *NC*, noncoronary.

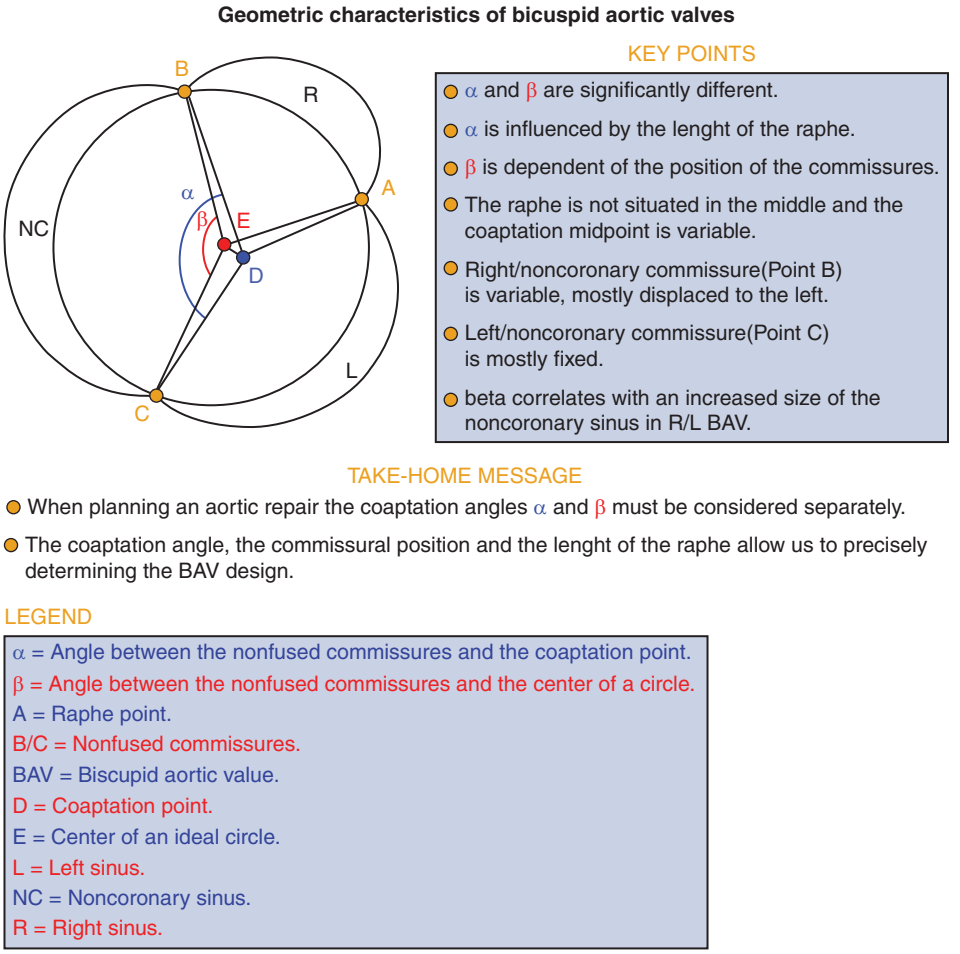

FIGURE 3. The coaptation angle α was measured starting from the central coaptation point D. The angle α is measured with lines drawn from the coaptation point D through the 2 functional commissures B and C. The angle β was measured to geometric center E determined by the circle method. The circle is adjusted to contain the three commissures. The angle is measured with lines drawn from the center of the circle through the 2 functional commissures B and C.

coaptation angle, the commissural position, and the length of the raphe separately and then reassembling them back together can give new perspectives on assessing the BAV design. This study confirms that BAV anatomy is even less uniform than already described,[23] showing different lengths of the raphes even in completely fused cusps, commissural positions, and relative dimensions of sinuses.

Further studies, including long-term follow-up and 4-dimensional flow magnetic resonance imaging, are needed to test whether these parameters are useful in BAV repair and whether these might have a beneficial influence on durable valve competence.

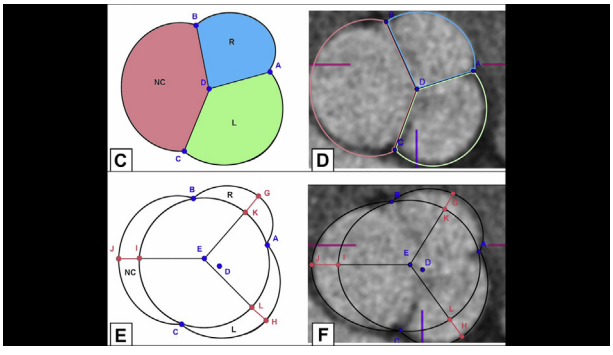

VIDEO 1. In the video, an author explains the main features of the study. Video available at: https://www.jtcvs.org/article/S2666-2507(21)00591-5/fulltext.

Conflict of Interest Statement

The authors reported no conflicts of interest.

The *Journal* policy requires editors and reviewers to disclose conflicts of interest and to decline handling or reviewing manuscripts for which they may have a conflict of interest. The editors and reviewers of this article have no conflicts of interest.

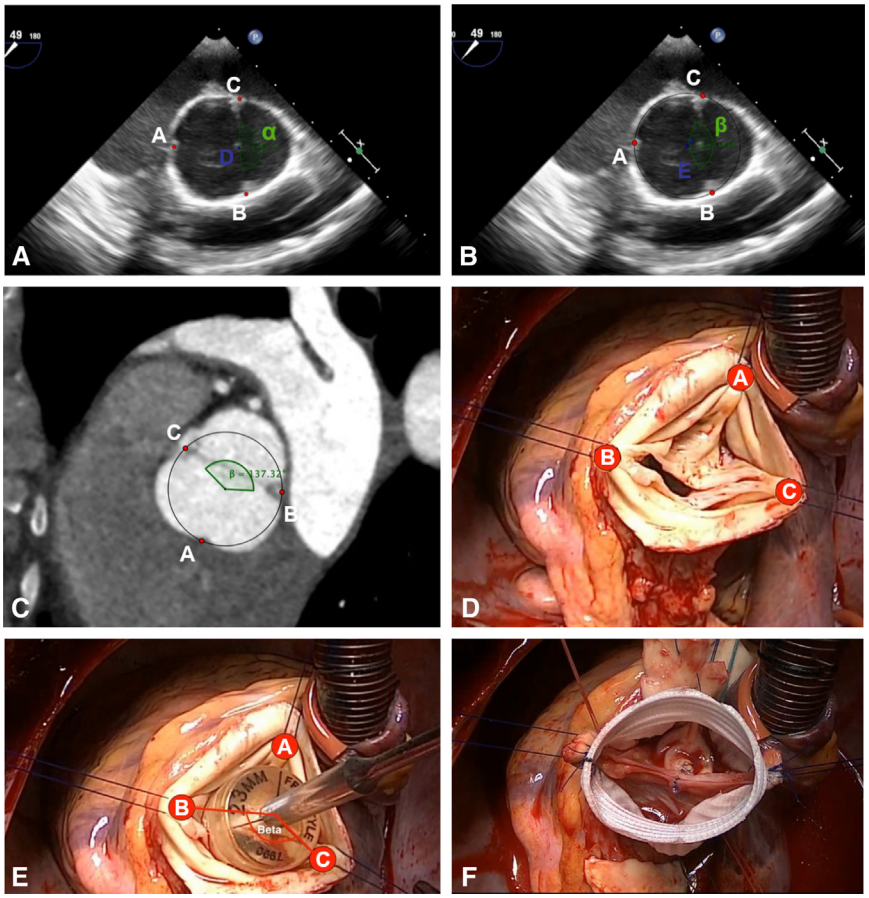

FIGURE 4. Application of the method described during an aortic valve repair of a bicuspid aortic valve with right/left fusion pattern. A, Measurement of angle α on tranesophageal echocardiography. B, Measurement of angle β on transesophageal echocardiography. C, Measurement of of angle β on computed tomography scan. D, Intraoperative view of the uninstrumented aortic valve. E, Intraoperative assessment of angle β with a valve sizer. F, Intraoperative view after root remodeling and valve repair without annuloplasty and without repositioning of the nonfused commissures.

References

1. Fedak PW, Verma S, David TE, Leask RL, Weisel RD, Butany J. Clinical and pathophysiological implications of a bicuspid aortic valve. *Circulation*. 2002; 106:900-4.
2. Ashikhmina E, Sundt TM III, Dearani JA, Connolly HM, Li Z, Schaff HV. Repair of the bicuspid aortic valve: a viable alternative to replacement with a bioprosthesis. *J Thorac Cardiovasc Surg*. 2010;136:1395-401.
3. Kari FA, Beyersdorf F, Siepe M. Pathophysiological implications of different bicuspid aortic valve configurations. *Cardiol Res Pract*. 2012; 2012:735829.
4. Vallabhajosyula P, Szeto WY, Komlo CM, Ryan LP, Wallen TJ, Gorman RC, et al. Geometric orientation of the aortic neoroot in patients with raphed bicuspid aortic valve disease undergoing primary cusp repair and a root reimplantation procedure. *Eur J Cardiothorac Surg*. 2014;45:174-80.
5. Aicher D, Kunihara T, Abou Issa O, Brittner B, Gräber S, Schäfers HJ. Valve configuration determines long-term results after repair of the bicuspid aortic valve. *Circulation*. 2011;123:178-85.
6. Padang R, Bagnall RD, Semsarian C. Genetic basis of familial valvular heart disease. *Circ Cardiovasc Genet*. 2012;5:569-80.
7. Schäfers HJ, Kunihara T, Fries P, Brittner B, Aicher D. Valve-preserving root replacement in bicuspid aortic valves. *J Thorac Cardiovasc Surg*. 2010; 140(Suppl):S36-40.
8. Schäfers HJ, Aicher D, Langer F, Lausberg HF. Preservation of the bicuspid aortic valve. *Ann Thorac Surg*. 2007;83:S740-5.
9. Mordi I, Tzemos N. Bicuspid aortic valve disease: a comprehensive review. *Cardiol Res Pract*. 2012;2012:196037.
10. Mazzitelli D, Stamm C, Rankin JS, Pfeiffer S, Fischlein T, Pirk J, et al. Leaflet reconstructive techniques for aortic valve repair. *Ann Thorac Surg*. 2014;98: 2053-60.
11. Joint Task Force on the Management of Valvular Heart Disease of the European Society of Cardiology (ESC), European Association for Cardio-Thoracic Surgery (EACTS), Vahanian A, Alfieri O, Andreotti F, Antunes MJ, et al. Guidelines on the management of valvular heart disease (version 2012). *Eur Heart J*. 2012; 33:2451-96.
12. Pettersson GB, Crucean AC, Savage R, Halley CM, Grimm RA, Svensson LG, et al. Toward predictable repair of regurgitant aortic valves: a systematic morphology-directed approach to bicommissural repair. *J Am Coll Cardiol*. 2008;52:40-9.
13. Aicher D, Schneider U, Schmied W, Kunihara T, Tochii M, Schäfers HJ. Early results with annular support in reconstruction of the bicuspid aortic valve. *J Thorac Cardiovasc Surg*. 2013;145(Suppl):S30-4.
14. Kari FA, Liang DH, Kvitting JP, Stephens EH, Mitchell RS, Fischbein MP, et al. Tirone David valve-sparing aortic root replacement and cusp repair for bicuspid aortic valve disease. *J Thorac Cardiovasc Surg*. 2013;145(3 Suppl): S35-40. e1-2.
15. Achenbach S, Delgado V, Hausleiter J, Schoenhagen P, Min JK, Leipsic JA. SCCT expert consensus document on computed tomography imaging before transcatheter aortic valve implantation (TAVI)/transcatheter aortic valve replacement (TAVR). *J Cardiovasc Comput*. 2012;6:366-80.
16. Ehrlich T, de Kerchove L, Vojacek J, Boodhwani M, El-Hamamsy I, De Paulis R, et al. State-of-the-art bicuspid aortic valve repair in 2020. *Prog Cardiovasc Dis*. 2020;63:457-64.

17. Abbas G, Danish A, Krasna MJ. Stereotactic body radiotherapy and ablative therapies for lung cancer. *Surg Oncol Clin N Am*. 2016;25:553-66.
18. de Kerchove L, Boodhwani M, Glineur D, Vandyck M, Vanoverschelde JL, Noirhomme P, et al. Valve sparing-root replacement with the reimplantation technique to increase the durability of bicuspid aortic valve repair. *J Thorac Cardiovasc Surg*. 2011;142:1430-8.
19. Lansac E, Di Centa I, Sleilaty G, Lejeune S, Khelil N, Berrebi A, et al. Long-term results of external aortic ring annuloplasty for aortic valve repair. *Eur J Cardiothorac Surg*. 2016;50:350-60.
20. Schäfers H-J, Schmied W, Marom G, Aicher D. Cusp height in aortic valves. *J Thorac Cardiovasc Surg*. 2013;146:269-74.
21. Lenz A, Petersen J, Riedel C, Weinrich JM, Kooijman H, Schoennagel BP, et al. 4D flow cardiovascular magnetic resonance for monitoring of aortic valve repair in bicuspid aortic valve disease. *J Cardiovasc Magn Reson*. 2020;22:29.
22. Efstratios I, Charitos H-HS. Anatomy of the aortic root: implications for valve-sparing surgery. *Ann Cardiothorac Surg*. 2013;2:53-6.
23. Sievers HH, Schmidtke C. A classification system for the bicuspid aortic valve from 304 surgical specimens. *J Thorac Cardiovasc Surg*. 2007;133:1226-33.

Key Words: aorta, aortic valve, bicuspid, aortic valve repair

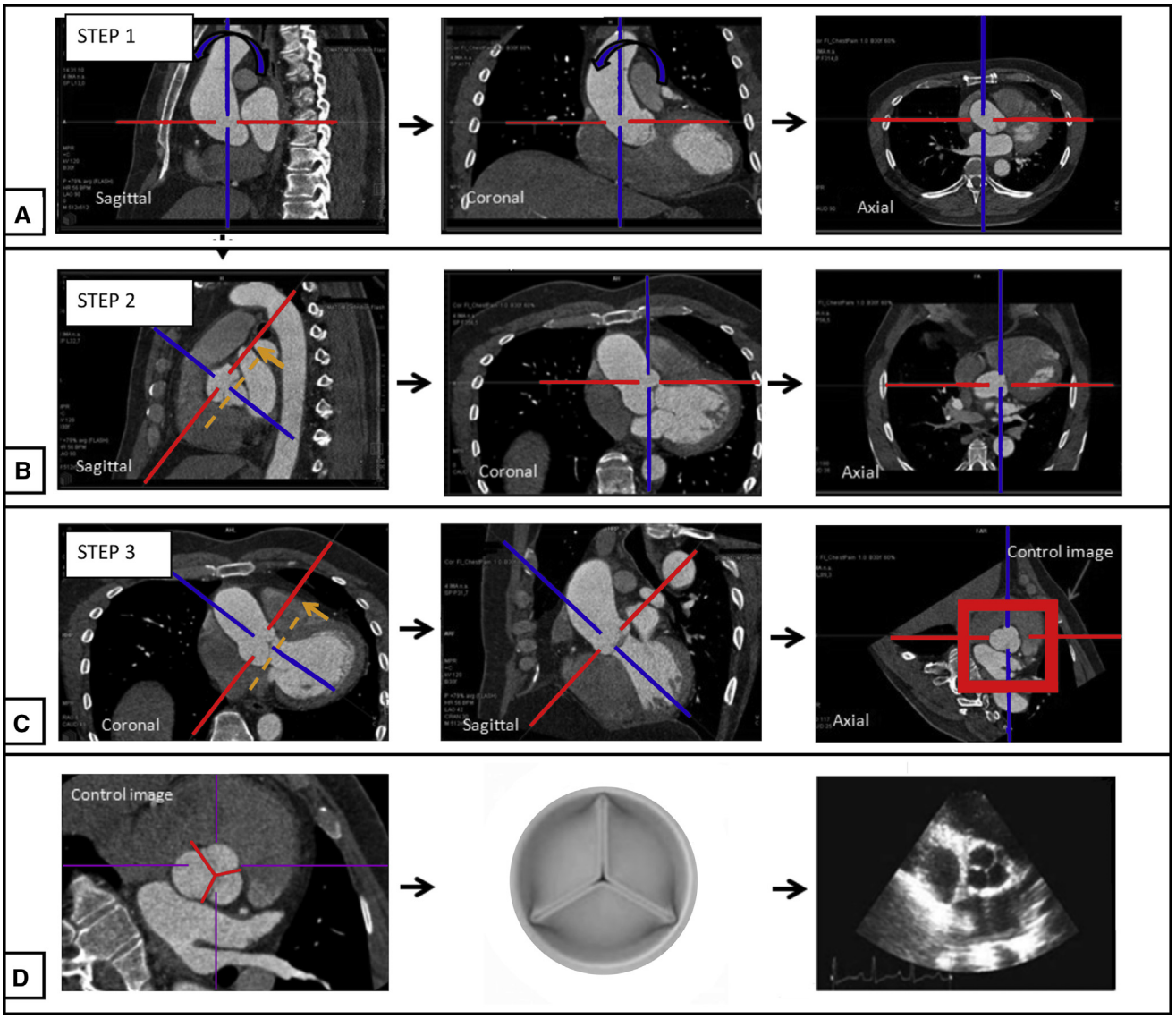

FIGURE E1. Description of the steps to create the desired image plane. Panel A: Step1: Multiplanar images in sagittal, coronal, and axial orientation are created to be simultaneously viewed to obtain the correct level in the axial orientation. Panel B: Step2: The sagittal and coronal images are rotated in the direction indicated by the arrows to obtain the right image plane of the aortic valve. The *red reference line* in the sagittal image is first used to rotate the view. This line approximates the level of the aortic annulus (*orange dotted line*). Panel C: Step 3: The procedure is repeated in the coronal image. Then, the computed tomography crosshair is moved upward, in cranial direction, to the level of maximal aortic sinus dimensions (*in accordance to the orange arrow*). These modifications also change the former coronal and axial images as displayed in sequence I. Panel D: Step 4: The axial image is checked to evaluate as whether this view corresponds with the clearest plane of the aortic valve. This control image is displayed in Panel D.

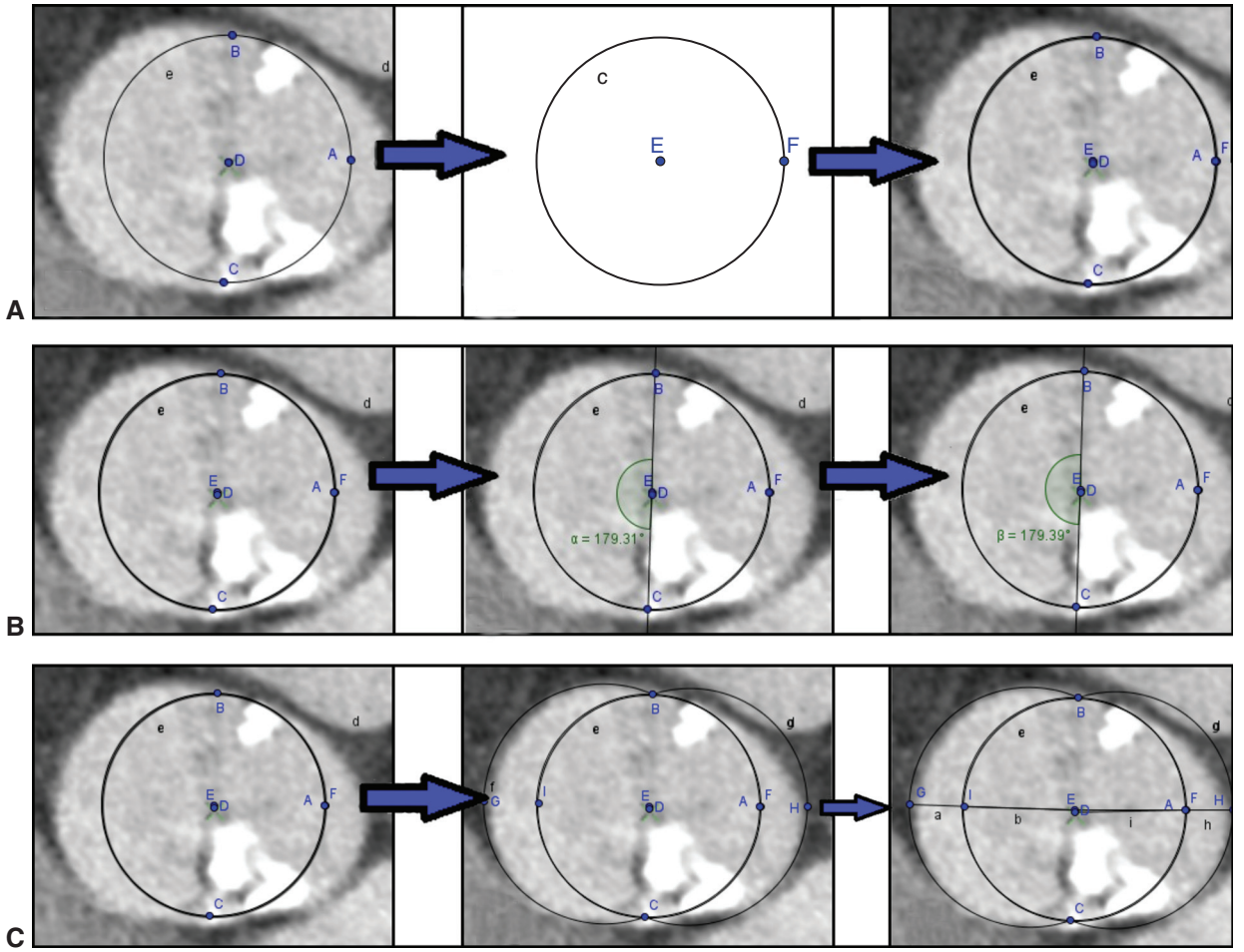

FIGURE E2. Method used in case of bicuspid aortic valve (BAV) with only 2 sinuses. Panel A: Upper Left, Fixed points are placed on the insertions of the non-fused commissures (B, C) and the central coaptation point (D). These valves contain no raphe, so only 2 points B and C can be used for creating a circle. Following geometrical rules, a circle cannot be created with only 2 points. Therefore, 2 opposite half circles are drawn through B and C, creating 1 circle (*upper middle*). The central point E was determined. The 2 circles are overlapped (*upper right*). Panel B: Angle α (BCD) and β (BED) are measured. The other angles are measured as for 3-sinus valves. Panel C: Measurement of relative aortic sinus dimensions: the 2 sinuses are indicated with arches. Fixed points are placed at the level of maximum sinus dimensions (points G and H). Then another series of fixed points are placed across from G and H, on the reference circle, respectively named I and F. From the center point E line sections are being drawn extending to G and H. These distance lines are determined. Then a next series of section lines are drawn from the same midpoint E to the opposite points I and also these distances are measured. These different dimensions are used to analyze relative to one another. The mathematical variations between the midpoints D and E are determined the same as applied in 3-sinus-valves using point A shown in the figure.

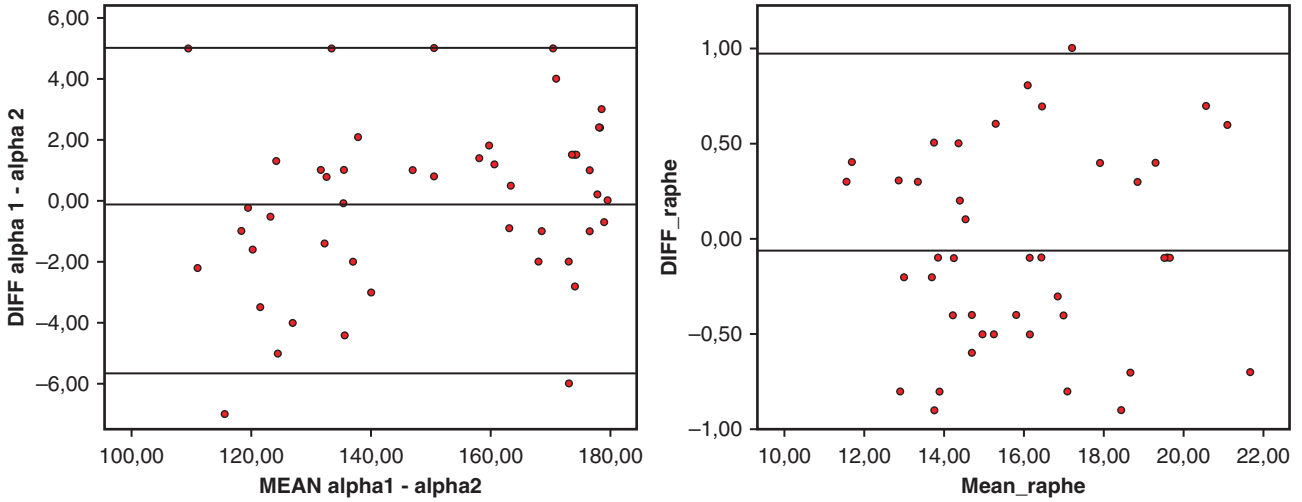

FIGURE E3. Bland-Altman plots and intrarater reliability. The *y*-axis illustrates the difference (*DIFF*) between the 2 measurements. The *x*-axis shows the means between the 2 repeated measurements.

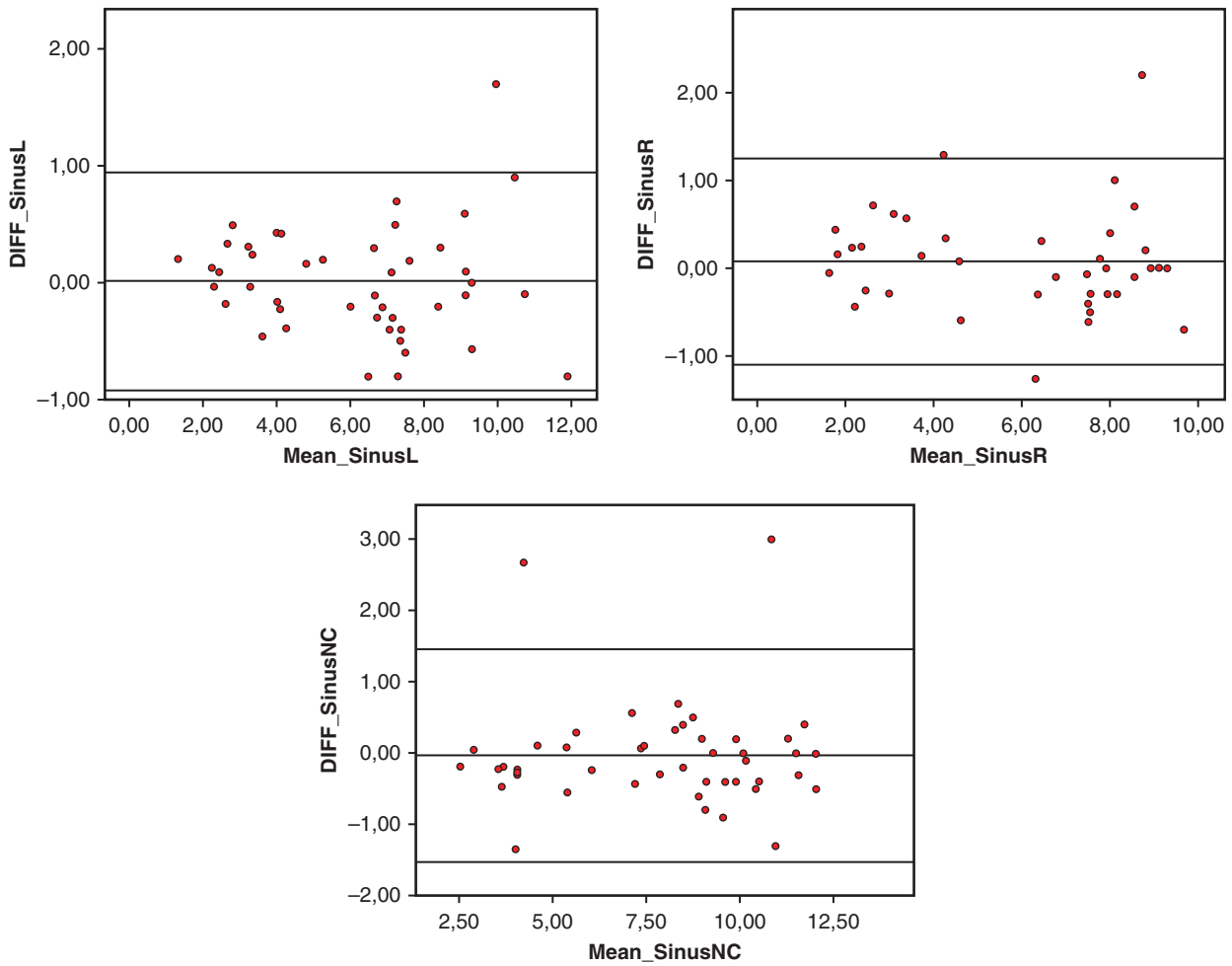

FIGURE E4. Bland-Altman plots and intrarater reliability. The *y*-axis illustrates the difference (*DIFF*) between the 2 measurements. The *x*-axis shows the means between the 2 repeated measurements. *L*, Left coronary; *R*, right coronary; *NC*, noncoronary.

TABLE E1. Aortic dimensions by subgroups (N = 45) as determine by computed tomography

Variable	Aorta dimensions (mm)						
	Men	Women	2 sinuses	3 sinuses	Right/left fusion pattern	Right/non fusion pattern	True
Annulus	27 (3.9)*	24 (7.0)	25 (3.0)†	27 (4.5)	27 (5.0)	27 (4.3)	25 (2.5)
Aortic root	40 (8.7)*	35 (16.0)	45 (13.0)†	35 (9.8)	35 (10.5)	40 (11.6)	36 (12.0)
STJ	34 (9.5)*	30 (5.8)	35 (12.5)†	32 (7.5)	31 (8.8)	36 (7.2)	35.2 (9.5)
Ascending aorta	43 (9.0)	41 (13.0)	50 (3.5)†	42 (10.0)	43 (10.5)	41 (9.5)	48 (9.7)
Aortic arch	28 (8.0)*	24.5 (5.5)	–	28 (5.5)	28 (5.2)	–	–

Values are presented as median (interquartile range difference) or as n (%). *STJ*, Sinotubular junction. *Significant versus women. †Significant versus 3-sinuses; annulus $P = .001$; aortic root $P = .015$; STJ $P = .002$; ascending aorta $P = .255$; aortic arch $P = .002$.

TABLE E2. Intraclass correlation

	Mean ± standard deviation	*P* value	ICC	*P* value	95% confidence interval
α_1-α_2	–0.13 ± 2.83	.152	0.996	.000	0.993-0.998
$LCraphe_1$-$LCraphe_2$	–0.06 ± 0.53	.719	0.989	.000	0.980-0.994
Sinus LC_1-Sinus LC_2	0.02 ± 0.48	.823	0.992	.000	0.986-0.996
Sinus RC_1-Sinus RC_2	0.08 ± 0.60	.646	0.987	.000	0.975-0.993
Sinus NC_1-Sinus NC_2	–0.04 ± 0.76	.982	0.988	.000	0.979-0.994

ICC, Intraclass correlation; *LC*, left coronary; *RC*, right coronary; *NC*, noncoronary.